AIAA JOURNAL
Vol. 46, No. 3, March 2008

Use of Material Tailoring to Improve Buckling Capacity of Elliptical Composite Cylinders

Miao Sun*
Virginia Polytechnic Institute and State University, Blacksburg, Virginia 24061
and
Michael W. Hyer†
AREVA NP Inc., Lynchburg, Virginia 24501

DOI: 10.2514/1.32495

Discussed is the importance of improvement of the axial buckling capacity of elliptical fiber-reinforced composite cylinders through material property tailoring by appropriately varying fiber orientation as a continuous function of circumferential position. The study is numerical in nature and relative to a baseline quasi-isotropic elliptical cylinder with the same geometry and the same number of composite layers, and therefore the same weight, increases in buckling capacity of 30% are predicted for what are considered small cylinders. Increases of 35% are predicted for larger cylinders. Several fiber angle variations with circumferential position are investigated, and each one results in improved buckling capacity. The scheme to determine the fiber angles as a function of circumferential position is based on an approximate buckling analysis of circular cylinders. Intralaminar material failure and postbuckling collapse of the cylinders are also investigated to determine if the material tailoring scheme has a detrimental effect on those responses. It is found that before collapse no material failure is predicted. Upon collapse, generally speaking, failures because of high stresses perpendicular to the fibers are more prevalent in the tailored designs than for the baseline quasi-isotropic case. However, with some tailored designs, no failures in the fiber direction are predicted, unlike the baseline case. Convergence of the numerical predictions is discussed, as is the effect of cylinder boundary conditions on the predicted improvement in buckling capacity.

I. Introduction

ALTHOUGH many cylindrical structures are based on a circular cross-sectional geometry, noncircular geometries may be required in certain applications. Blended wing-body aircraft designs, for example, may only be possible by considering noncircular fuselage cross sections. Aerodynamic and other geometric limitations could dictate noncircular cross sections for fuel tanks in launch vehicles. Unfortunately, there are structural disadvantages to a noncircular geometry. Because of the fact that the radius of curvature changes with circumferential location, there is what could be interpreted as a stress concentration effect at certain circumferential locations. The existence of increased stresses at specific circumferential locations is not particularly desirable, as the increased stresses can lead to material failure at these locations, both for high ultimate load levels as well as lower fatigue load levels. Furthermore, the changing radius of curvature makes specific circumferential locations more prone to buckle than other locations. Specifically, when a noncircular cylinder is subjected to an axial load, the cylinder buckles in the flatter portion of the cross section, while the deformations in the more highly curved portion of the cross section are practically nonexistent. This situation is illustrated in Fig. 1 for a simply supported fiber-reinforced composite cylinder with an elliptical cross section and a quasi-isotropic lamination sequence. The axial buckling load for this cylinder is 30–40% less than the axial buckling load of a quasi-isotropic circular cylinder with the same circumference. Similar characteristics are exhibited for cylinders constructed of other lamination sequences and of isotropic materials. The decreased buckling performance is because of the large radius of curvature associated with the flatter portion of the cross section. Equally important, however, is the fact that the decreased performance can also be viewed as being because of an inefficient or ineffective use of material. It would seem that the material properties of the cylinder could be tailored to involve the entire cylinder in the buckling phenomenon, perhaps increasing the axial buckling capacity. Since the radius of curvature varies in continuous fashion with the circumferential coordinate, it is logical that the material properties, particularly the stiffness, should also vary continuously with the circumferential coordinate.

One approach to achieving a continuous variation of stiffness with circumferential position when using fiber-reinforced composite materials is to control the fiber direction in a continuous fashion with circumferential position. Another option would be to vary the thickness of the cylinder wall with circumferential position. For the former approach, the basic challenge is to determine how fiber angles should be varied with circumferential positions so as to tailor the stiffness to increase the buckling capacity. It is the former concept that is the subject of this paper. Specifically, the objective of this paper is to demonstrate the development of a tailoring scheme based on variable fiber orientation so the buckling load of an elliptical cylinder is increased relative to a baseline noncircular design. Though an elliptical cross section is considered, the results obtained can be generalized to other noncircular cross sections such as an oval cross section. The postbuckling collapse behavior and material failure of the tailored elliptical cylinders are also of interest to determine if the proposed tailoring scheme has any adverse effect on those responses. Often stiffness tailoring comes with the loss of some other key property, and it is important to determine whether or not that is the case here.

To follow is a brief review of past work with noncircular cylinders. In the section following that the details of basic problem being considered, and for which the tailoring scheme is being developed, are presented, including cylinder geometry, material properties, and

Presented as Paper 2353 at the 48th AIAA/ASME/ASCE/AHS/ASC Structures, Structural Dynamics, and Materials Conference, Honolulu, HI, 23–26 April 2007; received 30 May 2007; revision received 18 August 2007; accepted for publication 18 August 2007.

*Engineer II, Structural and Fracture Mechanics Unit, 3315 Old Forest Road.

†N. Waldo Harrison Professor, Department of Engineering Science and Mechanics, Mail Code 0219. Fellow AIAA.

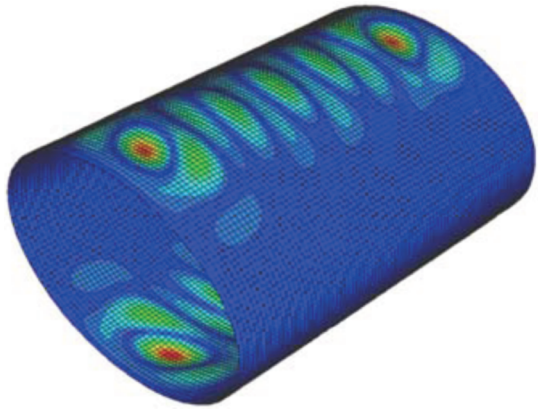

Fig. 1 Buckling deformations of simply supported quasi-isotropic cylinder with elliptical cross section.

boundary conditions. As most of the numerical results are based on using finite-element analyses, finite-element modeling of the problem is described. The subsequent section is a discussion of the quasi-isotropic elliptical cylinder illustrated in Fig. 1, which will be considered here as the baseline case. Then, it is postulated that a buckling analysis for circular cylinders can be used as a guideline for tailoring fiber angles with circumferential positions in elliptical cylinders so as to improve buckling capacity relative to this baseline case. This analysis of circular cylinders, which is approximate in nature and is essentially a classic approach, will be outlined in an appendix. Numerical results for the responses of several tailored cylinder designs are then presented and the results compared. The gains in buckling load that will be computed suggest that using a guideline that is based on the buckling analysis of a circular cylinder is a valid approach. To illustrate the robustness of the developed approach, cylinders with different overall dimensions and different boundary conditions are considered. Convergence of the numerical findings is also discussed. A summary of the findings and suggestions for future work are presented in the final section of the paper.

II. Brief Review of Past Work on Noncircular Cylinders

Soldatos [1] provided a comprehensive review of a number of investigations before 1999 that focused on noncircular cylinders. Relatively little activity with cylinders fabricated from composite materials was reported. Of the activity reviewed, vibration analyses were frequently cited, though some buckling results were reported [2–5], as were results for an internal pressure loading [6]. Firer et al. [7] developed an analysis by using a combination of Galerkin's method and the finite-difference technique to investigate behavior in the postbuckling range of axial loading. An important finding of their work was that imperfection sensitivity decreased with a decreasing cross-sectional aspect ratio, defined as the ratio of the minor diameter to major diameter. The sensitivity also depended on laminate configuration. Material failure was not addressed.

Since the time of the review, other investigations of noncircular composite cylinders have been reported. The influence of axial compression on composite cylinders with elliptical cross sections has been investigated experimentally [6] and numerically [8,9], including buckling and postbuckling [9]. Analyses have been conducted to investigate the influence of material orthotropy on the response of elliptical composite cylinders because of internal pressure [10] and a temperature change [11]. Numerical studies of the initial material failure of internally pressurized elliptical composite cylinders [12,13] have been conducted, as has a study of the influence of material orthotropy on failure progression and the potential for pressure-induced leakage [14]. In these studies the degree of material orthotropy was defined by the number of layers with fibers in the axial direction relative to the number of layers with fibers in the circumferential direction. In these investigations, material orthotropy was found to be an important parameter in determining stress and deformations levels in the cylinders, and hence influencing failure location and failure loading levels. This finding is important for the tailoring work discussed here because fiber directions (i.e., material orthotropy) will be changing continuously with circumferential position.

Torsional loading of quasi-isotropic elliptical cylinders, a loading that is most effectively resisted by a circular geometry, has been studied numerically quite recently [15]. Emphasis has been on postbuckling response, and the initiation and progression of failure. As with the other previously cited failure studies for elliptical composite cylinders [12–14], initial failure was predicted to occur at isolated circumferential locations because of the circumferentially varying stresses, again similar to a stress concentration effect. This is unlike the circular cylinders also investigated, in which failure was predicted to begin simultaneously at multiple locations around the circumference because of the axisymmetric geometry and loading. It is important to note that in these studies nitial failure was not always predicted to occur at the ends of the major or minor diameters. Also, surprisingly, initial failure was not always predicted to occur at the ends of the cylinder, as often happens because of boundary layer effects caused by the cylinder end conditions. Rather, in some cases initial failure was predicted to occur away from the ends. These observations are important, as a noncircular geometry, coupled with nonuniform material properties as proposed here, could result in unexpected effects, many of which could be beneficial.

Thomsen and Vinson [16,17] and Preissner and Vinson [18] investigated pressurized cylinders with cross sections that were almost rectangular, but rounded at the corners to relieve the stress concentration of a sharp square corner. The stresses in these rounded corners were clearly lower than if the corners were square, but much higher than in the flatter regions of the cross section. Also, the flatter regions were not particularly efficient reacting the pressure loading. This finding may have implications near the ends of the minor diameters of noncircular cylinders with small aspect ratios (e.g., 0.5), as the cylinder would be relatively flat at those locations.

Interestingly, the bending of orthotropic elliptical cylinders was the subject of an early investigation [19]. The orthotropy was because of stiffeners rather than material properties. As a matter of interest, it should be noted that there have been numerical investigations conducted on circular cylinders constructed such that the stiffness varied in the circumferential direction [20–22]. However, the stiffness variation considered in these particular studies was piecewise continuous in the circumferential direction rather than continuously varying, as the cylinders were constructed in segments in the circumferential direction.

III. Description of Basic Problem

The problem being considered is shown in Fig. 2, in which a composite cylinder with an elliptical cross section and subjected to a compressive axial displacement on one end, Δ, which is uniform with circumferential location, is illustrated. The opposite end of the cylinder is held fixed in the axial direction and the compressive axial displacement is increased in magnitude until buckling conditions are reached. Both simply supported and clamped boundary conditions at the cylinder ends are considered. The compressive load required to produce the compressive displacement is denoted as P. As shown, the major diameter, minor diameter, wall thickness, circumference, and length are denoted as $2a$, $2b$, H, C, and L, respectively. For purposes of discussion, the upper, lower, and side portions of the cross section are denoted as crown, keel, and sides, respectively. A circumferentially uniform axial displacement is a reasonable condition to consider. In a structure, circumferential stiffeners or bulkheads at the ends of a monocoque cylindrical section would enforce uniformity of displacements around the circumference. Also, a circumferentially uniform axial displacement would be a condition most likely enforced in any follow up experimental work. With a circumferentially uniform axial end displacement, the axial strain is essentially uniform in the circumferential and axial directions. Furthermore, an axial loading condition is among the simplest, and

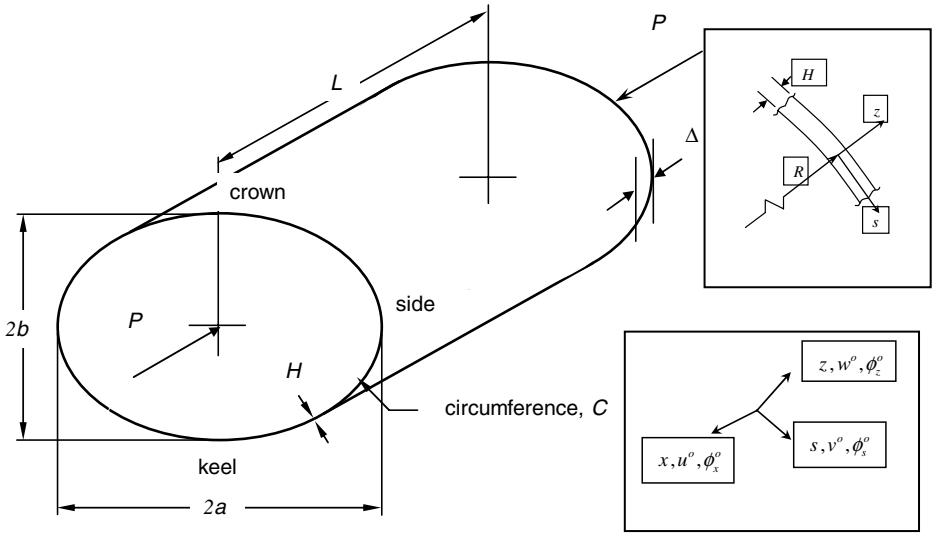

Fig. 2 Problem description, geometry, and nomenclature.

considering this loading condition provides a foundation for more complicated cases, including combined loads.

So as to determine the sensitivity of the response of cylinders constructed using the developed tailoring scheme to overall cylinder dimensions, two cylinder geometries are considered. These two cylinder geometries are listed in Table 1. Also listed in Table 1 for each cylinder geometry are the maximum and minimum radii of curvatures and the radius of a circular cylinder with the same circumference as the elliptical cylinder, R_o, a so-called equivalent circular cylinder. The eight-layer cylinder, referred to here as the small cylinder, has dimensions consistent with earlier experimental investigations [6,8] and numerical investigations, which addressed various aspects of the behavior of noncircular cylinders [13,14]. The other cylinder geometry, a 16-layer cylinder referred to here as the large cylinder, has a major diameter, minor diameter, and length five times larger than the small cylinder and is more representative of a structural scale than the small cylinder. The large cylinder is thinner, in the sense of $R_{\max}/H$, than the small cylinder, and hence more flexible. For both cylinders, the aspect ratio of the cross sections, b/a, is 0.7. Other aspect ratios are not investigated here, but it is believed that the approach to be discussed could be applied to other aspect ratios. The cylinders are assumed to be constructed of a medium modulus graphite-epoxy fiber-reinforced composite material. The elastic properties in terms of engineering constants in the principal material coordinate system, using standard notation for composite materials, and thickness of a single layer of material, h, are given in Table 1. Fabrication of a small tailored cylinder could conceivable be done by hand to provide specimens for initial experiments designed to further study the tailoring scheme developed. The large cylinder would require different fabrication techniques, presumable using tow placement equipment.

Table 1 Geometric and engineering properties used in calculations

Property (units)	Numerical value	
	Small cylinder	Large cylinder
a, m	0.1250	0.625
b, m	0.0875	0.438
L, m	0.320	1.600
$R_{\min}$, m	0.0613	0.307
$R_{\max}$, m	0.1786	0.890
R_0, m	0.1070	0.535
Wall thickness, H, mm	$8h = 1.120$	$16\,h = 2.24$
E_1, GPa	130.0	
E_2, GPa	9.70	
G_{12}, GPa	5.00	
ν_{12}	0.300	
Layer thickness, h, mm	0.1400	

The commercially available finite-element code ABAQUS was employed to compute numerical results. The SR4 shell element, a four-node quadrilateral element, with 6 degrees of freedom per node and employing reduced integration, was used. Details of the finite-element analysis coordinate system and the nodal degrees of freedom are illustrated in the insets in Fig. 2. The local radius to the middle surface of the cylinder is denoted as R, and the through thickness, or normal, coordinate as z. The axial and circumferential coordinates are identified as x and s, respectively. The translations and rotations associated with the x, s, and z directions of the middle surface are $u^o(x,s)$, $v^o(x,s)$, $w^o(x,z)$, $\phi_x^o(x,s)$, $\phi_s^o(x,s)$, and $\phi_z^o(x,s)$, respectively. Specification of simple-support and clamped-support boundary conditions in terms of the translations and rotations at the cylinder ends are as follows: For both support conditions,

$$\text{at } x=0\text{: } u^o=-\Delta, \quad v^o=0, \quad w^o=0, \quad \phi_x^o=0, \quad \phi_z^o=0$$
$$\text{at } x=L\text{: } u^o=0, \quad v^o=0, \quad w^o=0, \quad \phi_x^o=0, \quad \phi_z^o=0 \qquad (1)$$

while for simple-support conditions,

$$\text{at } x=0, L\text{: } \phi_s^o \text{ is unspecified} \qquad (2)$$

and for clamped-support conditions,

$$\text{at } x=0, L\text{: } \phi_s^o=0 \qquad (3)$$

For most calculations both large and small cylinders were modeled with 80 elements in the axial direction and 168 elements in the circumferential direction, for a total of 13,440 elements. Models with 160 elements in the axial direction and 336 in the circumferential direction, for a total of 53,760 elements, were used to check convergence characteristics. Those results will be discussed at the appropriate time. Geometrically nonlinear static analyses were conducted to study the prebuckling behavior of the cylinders to the axial compressive displacement, and to determine the onset of instability, which was assumed to occur when the level of axial displacement was such that the tangent stiffness matrix of the finite-element model was singular. Eigenvalue analyses based on a geometrically nonlinear prebuckling state were also used to study the onset of instability. These two approaches predicted nearly identical axial displacements for the onset of instability. Transient dynamic analyses were initiated at the onset of instability to determine the collapsed state of the cylinders. Regarding the transient dynamic analysis, in theory simply starting a dynamic analysis would have allowed the cylinder to move to another stable equilibrium configuration. However, this could have taken considerable amount

Table 2 Failure stress levels

Failure stress	σ_2^C	σ_1^T	σ_2^C	σ_2^T	τ_{12}^S
Value, MPa	1250	1500	200	50	100

of integration time, and hence computer time, and so instead, the cylinder was given a short duration, short amplitude pressure load (i.e., a pressure pulse), directed normal to the surface of the ellipse, to initiate cylinder motion. Specifically, over a 1 s time interval, the pressure increased linearly to 3500 Pa and then linearly to zero. A small amount of artificial damping was added to the dynamic analyses to hasten the convergence of the finite-element temporal integration procedure to the collapsed state. Such an approach was used successfully in past work [22].

Material failure was studied using the maximum stress failure criterion [23], which is based on uniaxial and shear failure stresses as measured in the principal material coordinate system. Here only intralaminar failure was considered and, using standard notation for stresses in the principal material coordinate system for a layer of fiber-reinforced composite material, the stresses of interest are denoted as σ_1, σ_2, and τ_{12}. The relevant failure stresses are denoted as

σ_1^T = tensile failure stress in 1-direction (i.e., the fiber direction)
σ_1^C = compressive failure stress in 1-direction
σ_2^T = tensile failure stress in 2-direction (i.e., transverse to the fiber direction)
σ_2^C = compressive failure stress in 2-direction
τ_{12}^S = shear failure stress in the 1–2 plane

The numerical values of these failure stresses for the graphite epoxy used in this study are given in Table 2. The equations associated with the maximum stress failure criterion are as follows:

Tensile failures ($\sigma_1 > 0$ or $\sigma_2 > 0$):

$$\frac{\sigma_1}{\sigma_1^T} = 1 \qquad \frac{\sigma_2}{\sigma_2^T} = 1 \tag{4}$$

Compressive failures ($\sigma_1 < 0$ or $\sigma_2 < 0$):

$$-\frac{\sigma_1}{\sigma_1^C} = 1 \qquad -\frac{\sigma_2}{\sigma_2^C} = 1 \tag{5}$$

Shear failure:

$$\frac{|\tau_{12}|}{\tau_{12}^S} = 1 \tag{6}$$

The stresses σ_1, σ_2, and τ_{12} in Eqs. (4–6) are computed at one integration point through the thickness of each layer in each element. These computed stresses are compared with the failure levels by way of Eqs. (4–6). Recall that there are 13,440 elements in the finite-element model, and the small cylinders consist of eight layers and the large cylinders of 16 layers. Therefore the calculations to study failure are performed on 107,520 integration points for the small cylinders and 215,040 integration points for the large cylinders. The failure mode at each integration point is determined by identifying which left-hand side of Eqs. (4–6) is equal to unity. The element number, layer number, and failure mode in which failures are detected are identified. Thus, a complete assessment of failure is made.

To evaluate the extent of damage that each cylinder experiences because of intralaminar material failure, two measures are used. One measure is based on the number of elements that experience failure in one or more layers, N_1, divided by the total number of elements in the finite-element model. The other measure is based on the number of integration points that experience failure, N_2, divided by the total number of the integration points in the finite-element model. Numerical values of these two measures of the extent of failure are presented for the various situations studied.

Table 3 Buckling values for simply supported quasi-isotropic elliptical cylinder[a]

Laminate	Δ_{cr}, mm	ε_{cr}, 10^{-3}	P_{cr}, kN
$[\pm 45/0/90]_S$	1.110	3.47	130.5

[a]Based on dimensions and material properties of small cylinder in Table 1.

IV. Numerical Results in Small Cylinders

In this section, numerical results for tailoring the material properties for the small cylinder geometry will be discussed. The baseline quasi-isotropic elliptical cylinder will be discussed first. The material tailoring scheme will then be described, and improved buckling results for various tailored cylinders presented.

A. Quasi-Isotropic Elliptical Cylinder: Baseline Case

The elliptical cylinder constructed of a quasi-isotropic lamination sequence and referred to in Sec. I, Fig. 1, is taken to be the baseline case for the results presented here. The specific quasi-isotropic lamination sequence is $[\pm 45/0/90]_S$. A quasi-isotropic laminate is fairly common, as the laminate material properties have little directional bias. Here that means that the effects of an elliptical geometry are not masked by material properties. Using the material properties and geometry for the small cylinder in Table 1, the buckling, or critical (cr), axial displacement, Δ_{cr}, average axial strain, ε_{cr}, and axial load, P_{cr}, of the small simply supported quasi-isotropic elliptical cylinder at the onset of instability are as given in Table 3. Herein, the axial strain is simply the axial displacement divided by the length of the cylinder, and so the axial strain is an average, or overall, value. The minus signs normally associated with compression are not used in Table 3. The configuration of the first buckling mode shape as determined from an eigenvalue analysis based on a geometrically nonlinear prebuckling equilibrium state is that of Fig. 1. The most obvious characteristic of the deformations illustrated in Fig. 1, as discussed, is that only the crown and keel portions of the cylinder participate in the buckling deformations. The sides of the cylinder are not involved. This characteristic is fundamental to elliptical cylinders, assuming the material properties do not vary with circumferential position. A second characteristic seen in Fig. 1 is the skewing of the deformation pattern because of the presence of the D_{16} and D_{26} stiffness terms in the bending stiffness matrix of the quasi-isotropic layup. The numerical values of the axial buckling strain and load in Table 3 will be used to normalize the to-be-discussed results for the tailored cylinders.

B. Material Tailoring Scheme

The lamination sequence of the eight-layer $[\pm 45/0/90]_S$ quasi-isotropic baseline elliptical cylinder is just one member of the laminate family $[\pm\theta/0/90]_S$, where for the quasi-isotropic case, $\theta = 45$ deg. The question posed is this: If the elliptical cylinder is constructed of this $[\pm\theta/0/90]_S$ lamination sequence, can the fiber angle θ be chosen to vary with circumferential position so the buckling performance of the cylinder is enhanced? The question is legitimate because the buckling behavior of a circular cylinder with a lamination sequence $[\pm\theta/0/90]_S$ depends strongly on the fiber angle θ and the radius of the cylinder. To gain insight into how the fiber angle θ might be varied, consider a circular cylinder of length L and radius R constructed of a $[\pm\theta/0/90]_S$ laminate. Using a buckling analysis for circular cylinders, the axial buckling strain, the axial buckling load, and other responses of interest can be computed. To put the calculations into context, it is useful to refer to Fig. 3, in which elliptical and circular cross sections are illustrated. For the elliptical cross section, the minimum radius of curvature, R_{min}, the maximum radius of curvature, R_{max}, and a radius of curvature at an arbitrary circumferential location, R, are shown. The accompanying circular cross section is chosen to have radius R, the radius of the elliptical cylinder at an arbitrary circumferential location. The radii of the circular cylinders to be studied with the buckling analysis, then, vary from $R = R_{min}$, representing a circular cylinder with the minimum

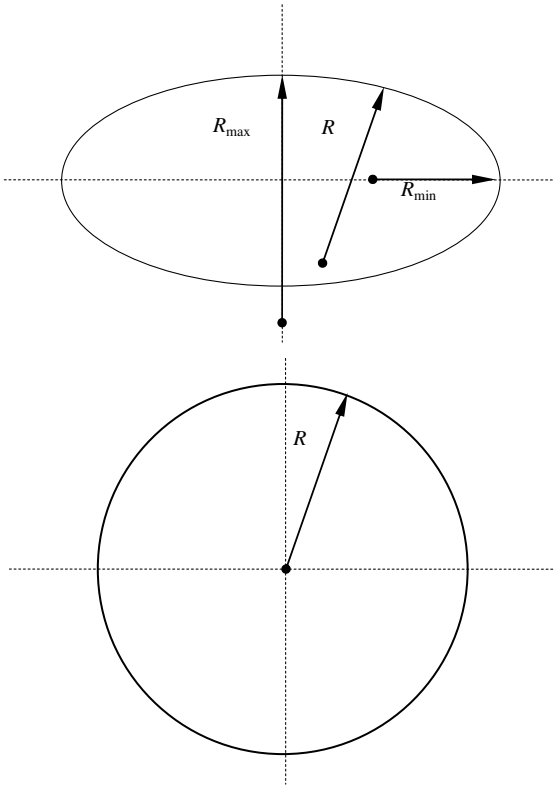

Fig. 3 Elliptical and circular cross sections.

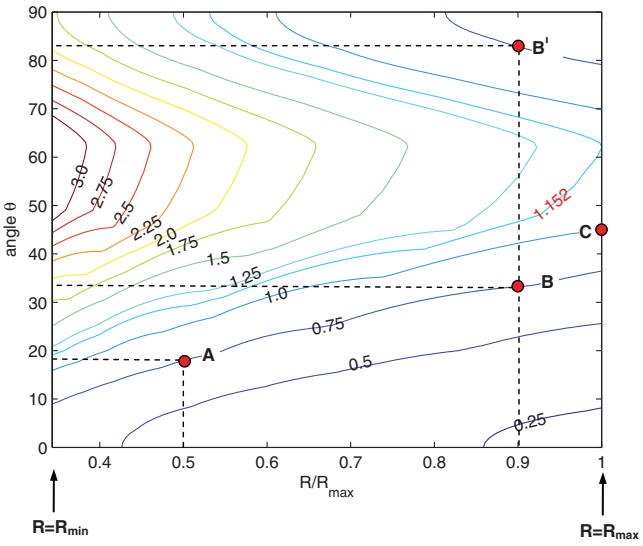

Fig. 4 Buckling strain contours as a function of radius for simply supported circular cylinders with lamination sequence $[\pm\theta/0/90]_S$ based on a simplified buckling analysis.

radius of curvature of the ellipse, to $R = R_{max}$, representing a circular cylinder with the maximum radius of curvature of the ellipse. The angle θ is allowed to vary from 0 to 90 deg, though laminates with fibers at the extremes of that range are not practical. The buckling strains of these circular cylinders can be computed as a function of radius R and angle θ of the laminate.

Here an approximate approach is used to compute the buckling strains of circular cylinders as a function of radius R and angle θ. The approximate approach assumes a circumferentially uniform axial displacement, a membrane prebuckling state, and simple-support boundary conditions. The approximate approach is briefly described in the Appendix. Results from this approximate analysis are summarized in Fig. 4, in which the horizontal axis is the radius of the circular cylinder, normalized by R_{max}, and the vertical axis is the layer angle θ in the laminate stacking sequence $[\pm\theta/0/90]_S$. Contours of buckling strain of the circular cylinders normalized by the buckling strain of the baseline quasi-isotropic elliptical cylinder of Fig. 1 and listed in Table 3 are identified. A number of interesting points can be made from Fig. 4. Point A, for example, represents the fact that for a circular cylinder with normalized radius of 0.5 and fiber angle θ of 18 deg (i.e., a circular cylinder constructed entirely of laminate $[\pm 18/0/90]_S$), the normalized buckling strain is 0.75. Likewise, point B represents the fact that for a circular cylinder with normalized radius of 0.9, a larger cylinder, and a fiber angle θ of 33 deg, the normalized buckling strain is also 0.75. Interestingly, because the contour line for a normalized strain of 0.75 has two branches, point B' represents the fact that the buckling strain for a cylinder with a normalized radius of 0.9, but a fiber angle θ of 83 deg, is also 0.75. This branch of larger angles will be referred to as the conjugate branch. To be noted is the fact that there are conjugate branches for some buckling strain levels and not others, and some buckling strain levels are valid only over a limited range of normalized radii. Also to be noted is that the normalized buckling strain of a quasi-isotropic circular cylinder with a maximum radius of curvature is unity, point C on the figure, where $\theta = 45$ deg. Since the normalization factor is the buckling strain of a quasi-isotropic elliptical cylinder, this is interpreted to mean that the buckling strain of the quasi-isotropic elliptical cylinder is equal to the buckling strain of a quasi-isotropic circular cylinder with a radius $R = R_{max}$ of the elliptical cylinder. This correlates well with the established relation for the so-called buckling stress of an isotropic elliptical cylinder [24] given as

$$\sigma_{cr} = \frac{EH}{R_{max}\sqrt{3(1-\nu^2)}} \tag{7}$$

The fact that the quasi-isotropic elliptical composite cylinder of Fig. 1 buckles only in the crown region, where $R = R_{max}$, also supports this equivalence.

To follow a particular strain contour over the range from R_{min} to R_{max} in Fig. 4 provides guidance for how to vary the fiber angle θ in the lamination sequence $[\pm\theta/0/90]_S$ as a function of radius of curvature for an elliptical cylinder. And since the radius of curvature and the circumferential location for an elliptical cross section can be related by geometry, the fiber angle θ as function of circumferential location can be specified so that the entire elliptical cylinder buckles at this level of axial strain. Strain is seen to be the key loading parameter in this particular problem because, as previously stated, with a circumferentially uniform axial displacement the strain is circumferentially and axially uniform. So yet another interpretation of the buckling pattern of Fig. 1 is that the strain level at the crown and keel regions is equal to the buckling strain level for those locations, while that same strain level represents a value less than the buckling levels for locations away from the crown and keel, that is, for locations with different local radii of curvature than the crown and keel. For that given strain level to represent a buckling level at locations away from the crown and keel, the lamination sequence must be different than it is at the crown and keel because the radii of curvature are different at those locations. If Fig. 4 is any sort of guide, several material tailoring schemes for this particular problem have essentially been prescribed which would lead to the entire cylinder participating in the buckling deformations at the critical level of axial displacement. Specifically, consider the normalized buckling strain level of 1.152. This level is close to the normalized buckling strain level of 1.0 for the quasi-isotropic elliptical cylinder in Fig. 1, and it is the maximum buckling strain level that can be achieved over the entire range of radii R_{min} to R_{max}; that is, the contour for 1.152 starts at the boundary $R = R_{min}$ and is just tangent to the boundary $R = R_{max}$. Using this contour, at the sides of the cylinder (i.e., at R_{min}), the fiber angle should be $\theta = 19$ deg, and at the crown and keel (i.e., at R_{max}), the fiber angle should be $\theta = 62$ deg. By the relation that relates the radius of curvature and circumferential coordinate for an ellipse, the fiber angle θ as a function of circumferential location between these

two circumferential locations can be determined for actual construction of the cylinder.

Another tailoring scheme of interest is the one associated with the conjugate branch for normalized strain level 1.152. For this branch, which represents the so-called tailored-conjugate cylinder, the fiber angles in the lamination sequence $[\pm\theta/0/90]_S$ are not a continuous function of circumferential location. Moving from the crown region (i.e., at $R = R_{\max}$), toward the side region (i.e., at $R = R_{\min}$), on the conjugate branch requires that at $R/R_{\max} \approx 0.53$, the fiber angle θ suddenly changes to that prescribed by the primary branch, a value of approximately 38 deg. So, to some extent, this case is not totally practical.

A third tailoring scheme of interest is the one associated with the normalized buckling strain of 1.0. For this case, at the crown and keel of the cylinder (i.e., at $R = R_{\max}$), the fiber angle is 45 deg. This tailoring scheme will be referred to as the quasi-isotropic crown case. For this case, the strain level of the tailored cylinder is the same as the strain level in the baseline quasi-isotropic cylinder, and in the crown and keel regions, the lamination sequence is a familiar one, namely, quasi-isotropic.

C. Buckling Performance of Tailored Designs

To determine if tailoring the fiber angle circumferentially based on Fig. 4 results in better buckling performance, a finite-element analysis of each the three tailoring schemes (i.e., tailored, tailored conjugate, and quasi-isotropic crown), was conducted using the finite-element model described previously. For the purpose of varying the fiber angle with the circumferential position, each quadrant of the elliptical cross section was divided into 14 equal-circumferential-length regions. With 168 elements in the circumferential direction, each quadrant consisted of 42 elements, and hence each of the 14 regions contained three finite elements. Within each region, the lamination sequence was $[\pm\theta/0/90]_S$, with θ fixed. The particular value of θ for each region, and hence for the three elements in the region, was taken from the $R/R_{\max}$ vs θ relation of Fig. 4 for each particular tailoring scheme by using the average radius for each equal-length region to select the value of θ. For the finite-element model, this was translated to fiber angle as a function of circumferential location. Of interest for each tailoring scheme were the buckling loads, the buckling mode shapes, postbuckling collapse behavior, and material failure. To provide a further comparison for the tailored designs, elliptical cylinders with lamination sequences $[\pm 19/0/90]_S$ and $[\pm 62/0/90]_S$, uniform with circumference, were considered. These two cases were considered because these laminates are at the extremes of the range of fiber angles for the 1.152 normalized strain level and it is plausible that they could out perform that tailored case. Simple-support boundary conditions were again considered.

The buckling strains and buckling loads for the various lamination sequences investigated are summarized in Table 4. The collapse loads to be discussed are also listed. The results have been normalized by the counterpart buckling values for the baseline quasi-isotropic elliptical cylinder of Fig. 1 and Table 3. Immediately obvious is that fact that all tailored designs result in increased buckling loads relative to the quasi-isotropic elliptical case. The tailored design using a normalized strain level of 1.152 results in nearly a 28% increase in buckling load, the tailored conjugate design 18%, and the quasi-isotropic crown design, which is based on a normalized buckling strain level of 1.0, nearly 30%. The quasi-isotropic crown cylinder exhibits more load capacity improvement relative to the quasi-isotropic cylinder, while being subjected to less axial compression strain than the tailored cylinder, because the overall axial stiffness for the quasi-isotropic crown cylinder is greater than that of the tailored cylinder. Overall, the fibers are more aligned with the axial direction for the quasi-isotropic crown case than for the tailored or tailored-conjugate designs. As a result, the axial load (strain multiplied by overall axial stiffness) for the quasi-isotropic crown design is greater than that for the case of tailored design. To be noted is that the buckling loads for the $[\pm 19/0/90]_S$ and $[\pm 62/0/90]_S$ cylinders are about 20 and 10% less than the baseline case, respectively. It should be noted that because the axial strain is simply the axial displacement divided by the cylinder length, normalized values of buckling axial displacement, though not shown, would be identical to the normalized values of the axial strain.

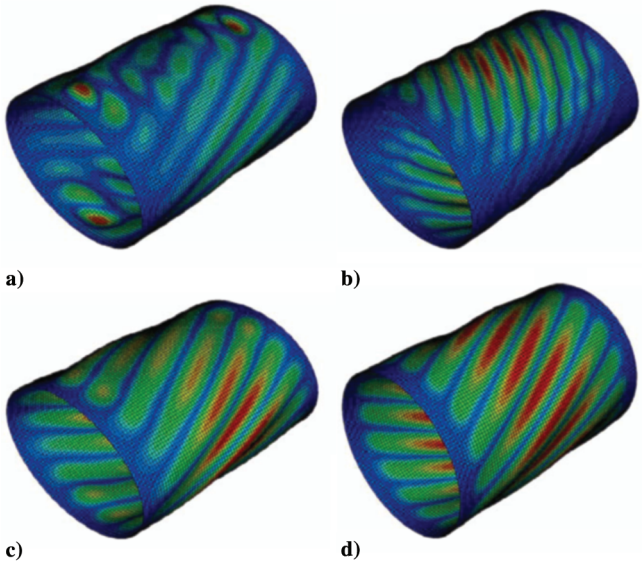

Fig. 5 Buckling mode shapes for a) tailored, b) tailored-conjugate, c) quasi-isotropic crown elliptical cylinders, and d) quasi-isotropic circular cylinder (first mode).

The buckling mode shapes for the various cases are illustrated in Fig. 5, including for comparison the buckling mode shape of a quasi-isotropic circular cylinder with the equivalent radius of curvature. What is immediately obvious from Fig. 5 is that buckling deformations of the three tailored designs, Figs. 5a–5c, encompass the entire cylinder, not just the crown and keel regions, just as is the case for the equivalent quasi-isotropic circular cylinder shown in Fig. 5d. The deformations of the tailored cylinder, Fig. 5a, form a short wavelength double-sinusoidal-like pattern in the axial and circumferential directions in the crown and keel regions, which transition into a more spiral-like pattern in the side regions. Those characteristics aside, the crown, keel, and side regions all participate in the buckling deformations. For the tailored-conjugate and quasi-isotropic crown cylinders, Figs. 5b and 5c, respectively, spiral-like deformation patterns encompass all circumferential locations. The buckling deformations of the quasi-isotropic crown case show a strong resemblance to the buckling deformations of the equivalent quasi-isotropic circular cylinder, Fig. 5d. It should be mentioned that the buckling deformations for the $[\pm 19/0/90]_S$ and $[\pm 62/0/90]_S$ cylinders (not shown) are confined to the crown and keel regions. Tailoring the lamination sequence so the entire cylinder is involved in the buckling process appears to be tantamount to increasing the buckling load. It is remarkable that the guidelines for tailoring derived from Fig. 4 are as good as they are. The normalized buckling strain levels for the three tailored elliptical cylinders computed using the previously described many-degree-of-freedom geometrically nonlinear finite-element model coincide very closely with the two normalized buckling strain levels selected from Fig. 4, which are based a simplified analysis of circular cylinders. Specifically, the variation in fiber orientation for the tailored and tailored-conjugate cylinders was based on a normalized buckling strain of 1.152 and on a buckling strain of 1.0 for the quasi-isotropic crown cylinder. The finite-element results predicted the tailored, tailored-conjugate, and quasi-isotropic crown designs would have buckling strains of 1.056, 1.094, and 0.977, respectively. These numbers represent less than a 10% difference between the buckling strains selected from the simplified analysis of Fig. 4 and the buckling strain levels actually computed by the much more refined finite-element analysis. It is clear the results in Fig. 4 can be used to address the negative effects of the noncircular geometry in a very fundamental way.

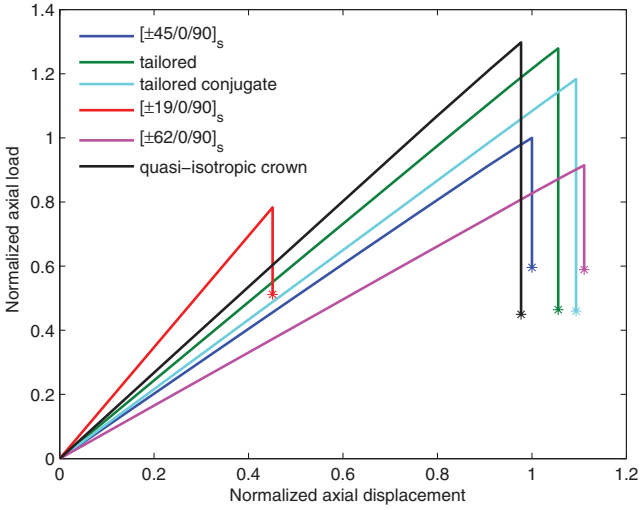

Fig. 6 Load vs end-shortening relations for elliptical composite cylinders.

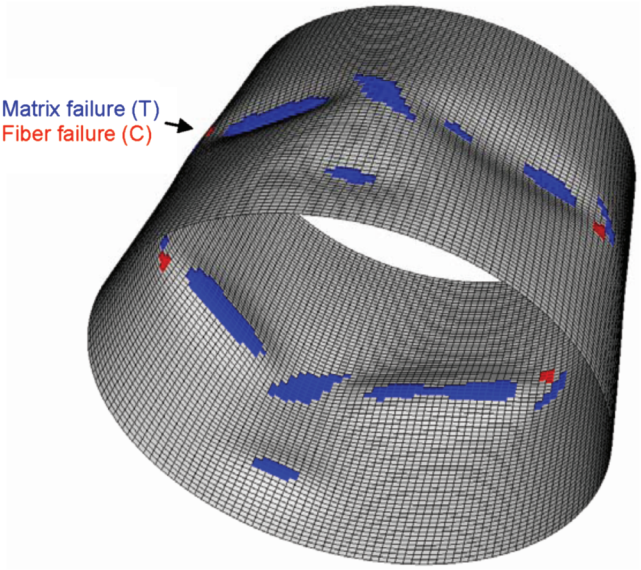

Fig. 7 Collapse deformations and failure characteristics of quasi-isotropic elliptical cylinder.

D. Collapse Deformations and Material Failure Characteristics

With the cylinders in an unstable state at the buckling level of axial displacement, a dynamic analysis was initiated with the end axial displacement held fixed at Δ_{cr} so the cylinder would move to a stable configuration at that level of axial displacement. This stable configuration will be referred to as the collapsed state of the cylinder. With this transition from the unstable configuration to a stable configuration, the axial load decreases. That is, the axial load required to hold the cylinder in the collapsed state at the buckling level of axial displacement is less than the axial buckling load. This is illustrated in Fig. 6, in which the axial load vs axial displacement relationships for the various cylinders, commonly known as the load vs end-shortening relations, starting from the zero level of axial displacement, are shown. In Fig. 6 the loads and axial displacements have been normalized by the counterpart values for the baseline quasi-isotropic elliptical cylinder. The load vs axial displacement relations for the cylinders are all very nearly linear up to the point of collapse (i.e., the sudden decrease in load). A close inspection of the relationships, however, reveals that for some cylinders there is a slight softening of the response as the buckling condition is approached. That the relationship is a vertical line at collapse is a consequence of fixing the axial displacement at the buckling value during the dynamic analysis and allowing the cylinder deformations and axial load to vary with time until a statically stable equilibrium configuration is reached. An alternative analysis would be to fix the load at the buckling level during collapse and allow the cylinder deformations and axial displacement to vary with time until a different statically stable equilibrium was reached. The former approach is taken because laboratory loading fixtures can be made to simulate the fixed displacement condition easier than the fixed load condition by the nature of the hydraulic or screw drive mechanisms common on loading frames. With fixed load conditions these mechanisms would have to accommodate large axial end displacement increases over a relatively short period of time. The peak load values of the relationships and the load levels at the lower end of the vertical lines correspond to the buckling and collapse values, respectively, given in Table 4. Also, the horizontal locations of the vertical lines correspond to the normalized axial strains in that table.

Throughout the axial displacement range of Fig. 6, the maximum stress failure criterion was used to determine if material failure was an issue. No failures were predicted to occur within any of the cylinders for displacement levels up to and including the buckling level. Upon collapse, however, material failure was predicted for all cylinders, and the nature and extent of failure varied from cylinder to cylinder. The deformed shapes and material failure characteristics of the six cylinders in their collapsed state are illustrated in Figs. 7–12. The locations and modes of failures are identified by shading the finite elements in which material failures were predicted. As observed in the figures, the deformed shapes of the collapsed cylinders are generally characterized by multiple inward dimples and outward ridges between the dimples. Failures occur around the dimples and ridges, but not elsewhere within the cylinder; for example, failures do not occur at or near the boundaries in which the displacements are restrained by the boundary conditions, a situation that can result in high stresses. In Table 5, other details regarding the failures are provided. The number of elements that are predicted to fail because of compression in the 1-direction ($-\sigma_1$), referred to here as fiber compression failure, tension, or compression in the 2-direction (σ_2 or $-\sigma_2$), referred to here as matrix tension or compression failure, and shear failure (τ_{12}), are listed. These numbers add to produce the values of N_1 and N_2, the parameters defined earlier to quantify the extent of failure within the cylinders. There were no predicted tensile failures in the 1-, or fiber-, directions.

For the quasi-isotropic baseline elliptical cylinder as illustrated in Fig. 7, the dimples ring the circumference at the midlength location and are deepest partway between the crown/keel and the sides. Because of the existence of the bending-twisting stiffness

Table 4 Comparison of buckling results for simply supported elliptical cylinders

Laminate	Normalized buckling strain or displacement[a]	Normalized buckling load[b]	Normalized collapsed load[b]
Quasi isotropic $[\pm 45/0/90]_S$	1	1	0.596
Tailored	1.056	1.279	0.464
Tailored conjugate	1.094	1.183	0.460
Quasi-isotropic crown	0.977	1.297	0.450
$[\pm 19/0/90]_S$	0.451	0.783	0.512
$[\pm 62/0/90]_S$	1.111	0.915	0.589

[a]Normalized by the buckling strain and displacement for the $[\pm 45/0/90]_S$ case in Table 3.
[b]Normalized by the buckling load for the $[\pm 45/0/90]_S$ case in Table 3.

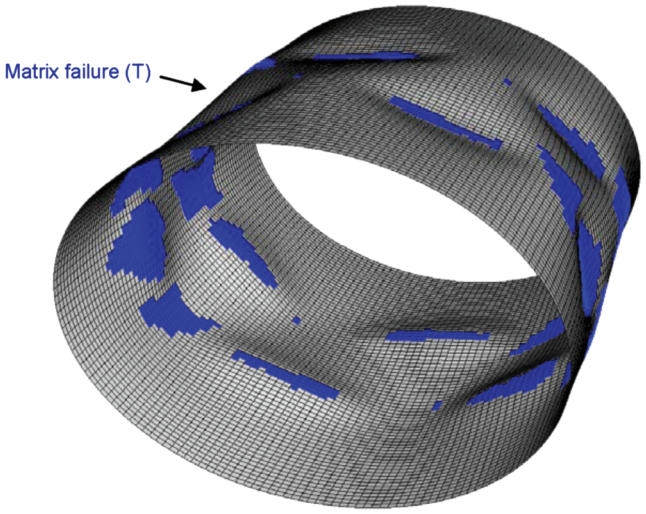

Fig. 8 Collapse deformations and failure characteristics of tailored elliptical cylinder.

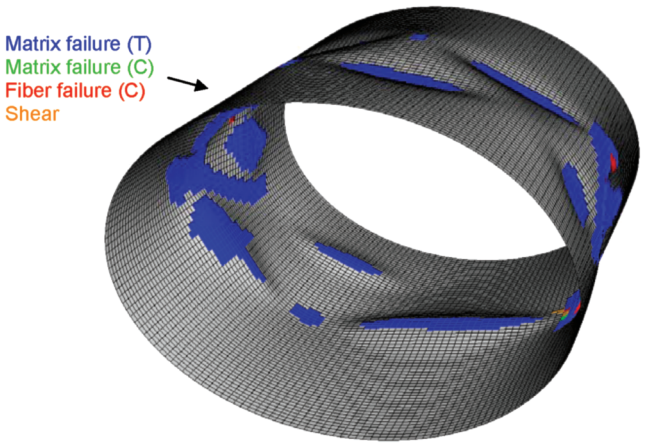

Fig. 9 Collapse deformations and failure characteristics of tailored-conjugate elliptical cylinder.

components in the laminate stiffness matrix, D_{16} and D_{26}, perfect symmetry of the collapsed configuration deformation pattern should not be expected. For the quasi-isotropic baseline case, the inward dimples are over eight cylinder wall thicknesses in depth and the ridges are over four wall thicknesses outward in magnitude. As observed in Fig. 7, matrix tension failures (T, blue) are generally predicted to occur wherever there is a dimple or ridge. Fiber compression failures (C, red) are also predicted to occur in the vicinity of dimples and ridges, but only near the sides of the cylinders. The matrix tension failures occur in the inner layer of the cylinder in the dimples and in the outer layer near the ridges because of the high tensile bending stresses at those through-thickness locations. Likewise, the fiber compression failures occur on the compression side of the dimple or ridge. However, these failures occur only near the sides because the smaller radii of curvature near the sides resist deformation, and so larger stresses are involved when dimpling does occur in those locations. Where the radius of curvature of the cylinder wall is larger, the fiber compression stresses are too low to cause material failure. Referring to Table 5, and as can be determined from Fig. 7, matrix tension failures contribute significantly to the extent of damage, though overall, based on the values of both N_1 and N_2, the extent of this damage is small. When the values of N_1 and N_2 are equal or nearly equal, as is the case with the quasi-isotropic cylinder, the failures occur in only one layer of each shaded element in Fig. 7.

The dimple pattern for the tailored cylinder shown in Fig. 8 consists of two rings of dimples, and accompanying ridges, that

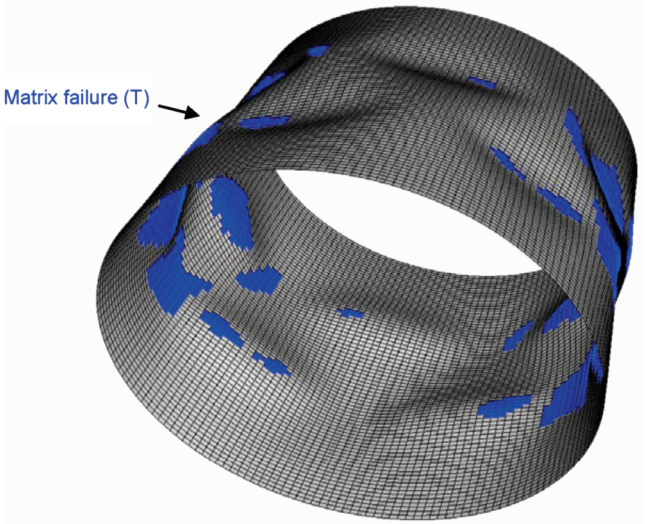

Fig. 10 Collapse deformations and failure characteristics of quasi-isotropic crown elliptical cylinder.

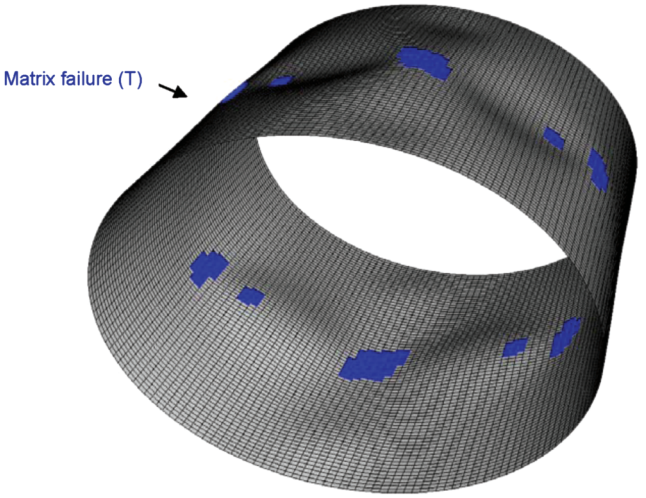

Fig. 11 Collapse deformations and failure characteristics of $[\pm 19/0/90]_S$ elliptical cylinder.

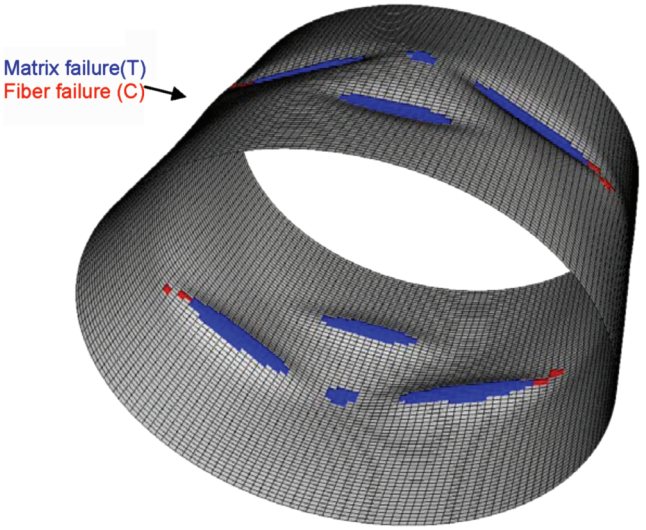

Fig. 12 Collapse deformations and failure characteristics of $[\pm 62/0/90]_S$ elliptical cylinder.

Table 5 Failure predictions for simply supported elliptical cylinders

Failure mode			N_1[a]	N_2[b]	% failure based on N_1[c]	% failure based on N_2[d]
Quasi isotropic	1-dir	$-\sigma_1$	23	23	0.1711	0.0214
	2-dir	σ_2	476	477	3.54	0.444
	shear	none	0	0	0	0
		total % failure			3.71	0.465
Tailored	1-dir	none	0	0	0	0
	2-dir	σ_2	1839	2539	13.68	2.36
	shear	none	0	0	0	0
		total % failure			13.68	2.36
Tailored conjugate	1-dir	$-\sigma_1$	41	41	0.305	0.0381
		σ_2	1790	2676	13.32	2.49
	2-dir	$-\sigma_2$	4	4	0.0298	0.00372
	shear	τ_{12}	5	5	0.0372	0.00465
		total % failure			13.69	2.54
Quasi-isotropic crown	1-dir	none	0	0	0	0
	2-dir	σ_2	1833	2566	13.64	2.39
	shear	none	0	0	0	0
		total % failure			13.64	2.39
$[\pm 19/0/90]_S$	1-dir	none	0	0	0	0
	2-dir	σ_2	376	376	2.80	0.350
	shear	none	0	0	0	0
		total % failure			2.80	0.350
$[\pm 62/0/90]_S$	1-dir	$-\sigma_1$	28	28	0.208	0.0260
	2-dir	σ_2	453	548	3.37	0.510
	shear	none	0	0	0	0
		total % failure			3.58	0.536

[a]Number of elements with at least one failed layer.
[b]Number of failed integration points.
[c]N_1 divided by the total number of elements $(13,440) \times 100\%$.
[d]N_2 divided by the total number of integration points $(107,520) \times 100\%$.

exhibit somewhat less deformation than the quasi-isotropic baseline case. Specifically, the dimples are slightly greater than six wall thicknesses in depth and the ridges just under three. Also, there are six dimples in each ring of dimples, as opposed to just four dimples for the single ring of dimples for the baseline case. The failure characteristics of the tailored cylinder are interesting in that no fiber failures are predicted. Based the values of N_1 and N_2 in Table 5, there are, however, considerably more matrix tension failures than for the baseline quasi-isotropic case. And, since N_2 is greater than N_1, at a given location more than one layer is experiencing the increased level of matrix tension failures. Of course, the prediction of no fiber failures for the tailored case depends strongly on the failure stress levels used in Table 2 and the failure criterion employed. Lower failure stress levels and/or an alternative failure criterion would no doubt show different results. However, the results suggest that for the tailored designs at collapse the fibers are stressed less than for the baseline quasi-isotropic case. This could be because of the lower collapse load level for the tailored case than for the quasi-isotropic case, or this could be because of the tailored nature of the fiber direction. This issue was not pursued. However, the characteristic is encouraging.

The tailored-conjugate cylinder, illustrated in Fig. 9, also has two rings of dimples, but the dimples are not as round in shape as those for the baseline and tailored cylinders. Referring to Fig. 4, it is seen that moving along the conjugate branch from the crown/keel regions, where the radius of curvature is a maximum, to the side regions of the cylinder, where the radius of curvature is a minimum, the fiber angle θ becomes 90 deg partway between the crown/keel and sides before suddenly changing to a smaller angle. Fiber angles near 90 deg result in a cylinder wall that has little axial stiffness partway between the crown/keel and sides. This low stiffness is believed to be responsible for the more creaselike form of the dimples seen in Fig. 9 as compared with the rounder form of dimples seen in Figs. 7 and 9. Compared with the baseline and tailored cylinders, the creaselike dimples are deeper and the ridges more outward; that is, slightly greater than nine and greater than four wall thicknesses, respectively. It is the formation of the dimples and ridges, or creases and ridges as the case may be, in all of the cylinders that is directly responsible for drop in axial load. In the regions of the dimples and ridges, the cylinder wall resists the axial load only through bending. Elsewhere, the cylinder wall resists the axial load through membrane action, a much more effective use of material stiffness. With a portion of the cylinder wall deformed with rather large dimples and ridges, the axial load that can be supported is much less than if there were no dimples or even minimum inward or outward deformations, which is the case just before collapse. Comparing values of N_1 and N_2 in Table 5, it is observed that the tailored-conjugate cylinder experiences much the same failure level at collapse as the tailored cylinder, as can also be seen in Fig. 9. However, for the tailored conjugate, more failure modes develop at collapse, including shear. As with the tailored cylinder, matrix tension failures occur in the inner and outer layers at the low and high points of all the dimples and ridges. Matrix compression failures, fiber compression failures, and shear failures occur at the sides, though the locations of these failures may be difficult to see because they occur over such small regions compared with the regions experiencing matrix tension failure.

The collapse deformations for the quasi-isotropic crown cylinder, depicted in Fig. 10, consist of two rings of dimples that are just over six wall thicknesses in depth and outward ridges that are just under three wall thicknesses outward. The deformation pattern is quite similar to that of the tailored case of Fig. 8. Based on the values of N_1 and N_2 in Table 5, failures at collapse in tailored cylinder with the quasi-isotropic crown are at much the same level of as in the two other tailored cylinders. Like the tailored cylinder, there are no fiber failures, only matrix tension failures, with more than one layer experiencing failure at various locations. As with the past cases, these matrix tension failures occur mostly in the low points of the dimples, with a few at the high points of the ridges. Recall, this cylinder was designed to have the same buckling strain level as the baseline case (normalized value of 1.0), yet it has 30% more buckling capacity. Its collapse load is the lowest of the cylinders investigated.

For completeness of the discussion, the collapse deformations and material failure characteristics for the $[\pm 19/0/90]_S$ cylinder are illustrated in Fig. 11 and those for the $[\pm 62/0/90]_S$ cylinder in

Fig. 12. The deformations of the $[\pm 19/0/90]_S$ resemble those of the quasi-isotropic baseline case, with four round dimples in a single circumferential ring that are under six wall thicknesses in depth, with accompanying ridges just over three wall thicknesses in magnitude. The creaselike dimples of the $[\pm 62/0/90]_S$ cylinder resemble those of the tailored-conjugate cylinder, though there are not as many, the creases again a result of the lack of axial stiffness of the $[\pm 62/0/90]_S$ lamination sequence. Interestingly, the collapse loads of the quasi-isotropic baseline case, with lamination sequence $[\pm 45/0/90]_S$, and the $[\pm 62/0/90]_S$ case are within a few percentage of each other, though the fiber angle θ is different by 17 deg for the two cylinders (see Table 4). It can be concluded from Fig. 11 that upon collapse, the $[\pm 19/0/90]_S$ cylinder only experiences matrix tension failures, the extent of failure being somewhat less than for the baseline quasi-isotropic cylinder. This is confirmed by the values of N_1 and N_2 in Table 5, where it is also confirmed that there are no fiber compression failures for this cylinder, and the extent of matrix tension failures is the least of any of the cylinders considered. On the other hand, the $[\pm 62/0/90]_S$ cylinder does exhibit fiber compressive failure, like the past cases in which fiber failure did occur, and matrix tension failures, mostly in the low points of the dimples and somewhat on the level of the baseline case. The fact that there are fiber failures for the $[\pm 62/0/90]_S$ cylinder, the baseline $[\pm 45/0/90]_S$ cylinder, and the tailored-conjugate cylinder suggests that when the fiber angles in the inner and outer layers are 45 deg or more, fiber compression failure is likely to occur near a dimple or ridge at or near the sides.

The results just presented suggest that material failure characteristics are not compromised by varying fiber orientation with circumferential position. There are, however, other issues to consider in this study before solid conclusions can be reached in this regard. These are discussed next.

V. Other Numerical Results

The dimensions of the elliptical cylinders discussed in the previous sections could be considered small, but gains by using tailoring were demonstrated, and they were substantial. It is important to determine whether similar gains can be obtained for larger cylinders using the same approach. Also, as with any study based on finite-element analysis, convergence of the results as it relates to discretization of the problem must also be considered. Finally, it is of interest to investigate the influence of tailoring for the case of clamped boundary conditions. Here the variation of θ with circumferential position determined for simply supported conditions is applied to cylinders with clamped boundary conditions to determine if gains similar to those computed for simple-support boundary conditions are predicted. These three issues are addressed in the following sections.

A. Consideration of Large Cylinders

To study the influence of tailoring on the large elliptical cylinders, the 16-layer lamination sequence $[\pm\theta/0/90]_{2S}$ is considered. For convenience of narration, hereafter the elliptical cylinders discussed in the previous section will be referred to as small cylinders, whereas the cylinders studied in this section will be referred to as large cylinders. Recall, the numerical values of the dimensions of the large elliptical cylinder and material properties were given in Table 1. A large quasi-isotropic elliptical cylinder with lamination sequence $[\pm 45/0/90]_{2S}$ is used as a baseline and for normalization. The strain contour characteristics for large circular cylinders (not shown) determined by the approach described in the Appendix are very similar to those illustrated in Fig. 4 for small circular cylinders. In fact, the contour analogous to the normalized strain level of 1.152 in Fig. 4 for the small cylinder has a normalized value of 1.224 for the large cylinder. The extremes of the fiber angle range for the large cylinders are 18 and 56 deg, compared with 19 and 62 deg for the small cylinders, similar values.

Table 6 Buckling values for quasi-isotropic elliptical cylinders

	Δ_{cr}, mm	ε_{cr}, 10^{-3}	P_{cr}, kN
small cylinder $[\pm 45/0/90]_S$	1.110	3.47	130.5
large cylinder $[\pm 45/0/90]_{2S}$[a]	2.25	1.408	530

[a]The major diameter, minor diameter, and length of the large cylinder are five times larger than for the small cylinder. The wall thicknesses differ by a factor of 2.

For the large elliptical cylinders, the finite-element approach used was identical to that for the small elliptical cylinders. The same mesh density and discretization of the fiber angle θ vs circumferential position using 14 regions was used. The computed buckling parameters for the large quasi-isotropic elliptical cylinder are presented in Table 6, in which the parameters for the small quasi-isotropic elliptical cylinders are presented for comparison. The ratios of the buckling strain and load for the small compared with the large quasi-isotropic elliptical cylinders are 2.46:1 and 1:4.06, respectively. For large and small isotropic equivalent circular cylinders (radii R_o given in Table 1) these ratios would be 2.5:1 and 1:4. The normalized buckling parameters and collapse loads for the three large tailored elliptical cylinders and the two large elliptical cylinders constructed with fixed fiber angles at the extremes of the range are presented in Table 7. From the results in Table 7 it can be said that there are certainly gains in buckling loads to be achieved with tailoring, and a comparison with Table 4 reveals that the gains are more than for the small cylinders. For example, relative to their respective baseline cylinders, the large tailored elliptical design shows a nearly 38% increase in buckling load compared with a nearly 28% increase for the small tailored elliptical design. Interestingly, the normalized collapse loads for all large elliptical cylinders are less than for the small elliptical cylinders.

The collapse deformations for the large cylinders (not shown), both tailored and nontailored, differ from those of the small cylinders in that there are more dimples, and accompanying ridges, in the larger cylinders. Like the small cylinders, however, the dimples and ridges form ring patterns around the circumference. The magnitudes of the dimples and ridges, relative to the wall thickness, are similar to those for the small cylinders. That there are more dimples and ridges for the large cylinders is believed to be responsible for the lower collapse load. With more dimples and ridges in the large cylinders, a higher portion of each cylinder is resisting the axial load with bending deformations compared with more effective membrane deformations. It is important to note that no material failures are predicted for the large quasi-isotropic, $[\pm 18/0/90]_{2S}$, or $[\pm 56/0/90]_{2S}$ cylinders. For all large tailored cylinders only matrix tensile failures, located near the sides, are predicted and to a lesser extent than for the small cylinders. For example, the percentage of failures as measured by the number of elements with at least one failed layer (N_1) is approximately 0.5% for the large tailored cylinder as compared with

Table 7 Buckling results for large simply supported elliptical cylinders

Laminate	Buckling strain (normalized[a])	Buckling load (normalized[b])	Collapsed load (normalized[b])
Quasi isotropic $[\pm 45/0/90]_{2S}$	1	1	0.544
Tailored	1.124	1.379	0.351
Tailored conjugate	1.162	1.280	0.326
Quasi-isotropic crown	0.980	1.357	0.378
$[\pm 18/0/90]_{2S}$	0.467	0.820	0.493
$[\pm 56/0/90]_{2S}$	1.149	0.984	0.528

[a]Normalized by the buckling strain for the $[\pm 45/0/90]_{2S}$ case in Table 6.
[b]Normalized by the buckling load for the $[\pm 45/0/90]_{2S}$ case in Table 6.

13.68% (Table 5) for the small tailored cylinder. The lack of fiber failures and the lower level of matrix failures is a reflection of the fact that the overall strain levels at buckling for the large cylinders are less than for the small cylinders.

B. Convergence Studies

With this problem there were two aspects to the question of convergence of the finite-element calculations. To this point in the discussion, as stated, the finite-element model used to compute the results consisted of 168 elements in the circumferential direction and 80 in the axial direction, for both the large and small cylinders. Furthermore, a one-quarter circumference of the cross section has been divided into 14 regions, three elements per region, and the tailored fiber angle θ has been taken to be constant in each region, and therefore the same in each of the three elements making up the region. To determine if dividing a one-quarter circumference into more constant-angle regions influenced the predicted buckling improvement levels for the tailored designs, each of the 42 elements per quarter circumference was considered a separate region, and the tailoring angle was varied on an element-by-element basis, thereby producing a three-fold level of refinement for defining the variation of θ with circumferential position. The calculations were done using the large cylinder geometry because for the larger cylinder a constant fiber angle region covers a larger circumferential length, physically, than for the smaller cylinder. Perhaps the use of a single value of θ over a large circumferential region may have undue influence on the results. Despite these concerns, for the tailored and tailored-conjugate cylinders, the buckling strain and buckling load computed using 42 regions were less than 1% different than the values computed using 14 regions. The buckling mode shapes and collapsed deformations were virtually identical, including the magnitude of the dimples and ridges. As measured by the values of N_1 and N_2, the degree of damage predicted by the 42-region model was 8% greater. This is not considered a significant difference. Basically, very low failure levels were predicted by both analyses, and it could be concluded that using 14 regions provided an accurate assessment of the effect of tailoring.

To address the issue of mesh density, again considering the large elliptical cylinder, the mesh density was doubled in both the circumferential and axial directions to create a 336×160 element model. Each of the 84 elements in a one-quarter circumference was considered a separate region for determining the tailored fiber angle θ, and so again the angle varied on an element-by-element basis. It should be mentioned that the difference in tailoring fiber angle from element to element, (i.e., from region to region), was less than 1 deg. This was considered to be a resolution that would be quite difficult to achieve when manufacturing tailored elliptical cylinders, but it was in keeping with the question of the influence of mesh and region refinement on the numerically predicted improvement in buckling load levels.

The predicted buckling strain and buckling load of the large tailored and tailored-conjugate elliptical cylinder using the 84-region model were less than 1% lower than the buckling load predicted by the less-refined mesh and the 14-region model. The collapse deformation patterns predicted by the 84-region model were much the same as those based on the coarser mesh and 14 regions, and the magnitudes of the dimples and ridges predicted using the 84-region model were within 7% of the magnitudes predicted using the 14-region model and the coarser mesh. The predicted level of damage at collapse, as measured by the values of N_1 and N_2, was again less than 8% different using the 84-region model as compared with using 14 regions and a less-refined mesh, and again, this difference was not considered significant. In summary, the convergence studies provided evidence that the qualitative and quantitative results and ensuing conclusions obtained using 14 regions and a less-refined mesh were valid.

Table 8 Buckling values for small quasi-isotropic elliptical cylinders with various boundary conditions

	ε_{cr}, 10^{-3}	P_{cr}, kN
clamped	3.59	136.5
simply supported	3.47	130.5

C. Clamped Boundary Conditions

It is well known that for circular cylinders with dimensions similar to those considered here, the boundary conditions do not have much influence on the buckling load. The same was true for elliptical cylinders discussed here. The specific numbers for a small clamped $[\pm 45/0/90]_S$ quasi-isotropic elliptical cylinder, as computed by the less-refined finite-element mesh, are given in Table 8. The results for the small simply supported $[\pm 45/0/90]_S$ quasi-isotropic elliptical cylinder from Table 3 are included for comparison. The buckling strain and load for the clamped cylinder are within 5% of those for the simply supported cylinder. To investigate the robustness of the tailoring concept developed, the tailored fiber angle variation θ vs circumferential location determined from Fig. 4, which, recall, is based on a simplified analysis of simply supported circular cylinders, was applied to the clamped elliptical cylinder. The buckling strains, buckling loads, and collapse loads for the various tailored and constant-angle clamped elliptical cylinders are given in Table 9. The buckling strains and loads in Table 9 have been normalized by like quantities for the clamped quasi-isotropic elliptical cylinder of Table 8, but also for consistency, and in an additional column, by the like quantities for the simply supported case. It can be concluded from Table 9 that the buckling loads for the tailored clamped elliptical cylinders show improvements of the level shown for the simply supported elliptical cylinders presented in Table 4. The calculations for the large cylinders (not shown) also indicate that the collapse deformations are not strongly influenced by the clamped boundary conditions, and the values of N_1 and N_2 for the clamped tailored and fixed-angle elliptical cylinders are within $\pm 15\%$ of the values for the simply supported cylinders.

VI. Conclusions and Discussion

The concept of tailoring material properties by varying fiber orientation with circumferential position in elliptical composite cylinders for the purpose of improving axial buckling capacity has been discussed. Improved buckling capacity was based on the notion that if the entire cylinder could be made to participate in the buckling

Table 9 Comparison of buckling results for small clamped elliptical cylinders

	Buckling strain		Buckling load		Collapsed load	
Laminate	Case 1[a]	Case 2[b]	Case 1[a]	Case 2[b]	Case 1[a]	Case 2[b]
Quasi isotropic, $[\pm 45/0/90]_S$	1	1.035	1	1.046	0.571	0.597
Tailored	1.075	1.112	1.298	1.358	0.445	0.465
Tailored conjugate	1.061	1.096	1.138	1.190	0.424	0.443
Quasi-isotropic crown	0.966	0.999	1.278	1.337	0.431	0.451
$[\pm 19/0/90]_S$	0.436	0.451	0.749	0.784	0.498	0.521
$[\pm 62/0/90]_S$	1.110	1.147	0.908	0.950	0.552	0.577

[a]Normalized by the clamped quasi-isotropic cylinder in Table 8.
[b]Normalized by the simply supported quasi-isotropic cylinder in Tables 3 and 8.

deformations, then axial buckling load would increase. The question of how to vary fiber orientation with circumferential position to achieve this was addressed by considering a simplified buckling analysis of circular composite cylinders. It has been shown qualitatively and quantitatively that improvements in buckling capacity can be achieved. Importantly, material failure characteristics are not compromised by varying fiber orientation with circumferential position. No failures were predicted, up to and including buckling for any cylinder studied. Upon collapse, material failure occurred in all of the small cylinders discussed, but for two of the small tailored cylinders, no fiber failures were predicted for the collapsed state. It was also demonstrated that the tailoring scheme worked for cylinders that were considerably larger in overall size. In addition, cylinders with clamped boundary conditions responded positively to the same fiber angle variation with circumferential location.

Though specific geometries and boundary conditions have been studied, there are broader implications to the findings that are important. First, it would appear that much of the axial buckling capacity that is lost by using an elliptical cross section rather than a circular cross section is regained by using the continuously varying fiber orientation. It is believed this could also be the case for other noncircular cylinders (e.g., cylinders with oval cross sections). Second, the convergence studies suggest that a coarse discretization of the fiber angle variation could be used to adequately study improvements when considering other noncircular cross sections or other loading conditions. Finally, the tailoring scheme is insensitive to boundary conditions, and so no matter how a cylinder is supported at the ends, gains in buckling capacity can be achieved.

Future activities should address other loading conditions, such as internal pressure and bending, and combined effects and other cross-sectional aspect ratios. It is also important to determine the sensitivity of the results to geometric or material imperfections in the cylinders. Perhaps most importantly, future activities must address the manufacturing elliptical cylinders with continuously varying fiber orientation.

Appendix: Approximate Buckling Analysis for Circular Cylinders

An elementary buckling analysis based on a Ritz approximate solution of the Trefftz stability criterion applied to circular cylinders of length L, radius R, and constructed of composite materials is described in this Appendix. The approximate solution assumes a membrane prebucklng state, and therefore no prebuckling rotations, and simple-support boundary conditions. The laminate constructions considered are symmetric and balanced. The Trefftz criterion is based on equating to zero the first variation of the second variation of the total potential energy, here denoted as π. Based on Donnell cylinder theory, and using notation common in the analysis of circular cylinders, the first variation of the second variation equated to zero can be written as

$$\begin{aligned}\delta(\delta^2\pi) = \int_x\int_\theta \Bigg\{ & N_{x1}\frac{\partial\delta u_1^o}{\partial x} + N_{\theta 1}\left(\frac{\partial\delta v_1^o}{R\partial\theta} + \frac{\partial\delta w_1^o}{R}\right) \\ & + N_{x\theta 1}\left(\frac{\partial\delta v_1^o}{\partial x} + \frac{\partial\delta u_1^o}{R\partial\theta}\right) + M_{x1}\frac{\partial\delta\beta_{x1}^o}{\partial x} + M_{\theta 1}\frac{\partial\delta\beta_{\theta 1}^o}{R\partial\theta} \\ & + M_{x\theta 1}\left(\frac{\partial\delta\beta_{\theta 1}^o}{\partial x} + \frac{\partial\delta\beta_{x1}^o}{R\partial\theta}\right) + (-N_{\rm cr})\beta_{x1}^o\delta\beta_{x1}^o\Bigg\} R\,{\rm d}\theta\,{\rm d}x = 0 \end{aligned} \tag{A1}$$

The subscript 1 refers to quantities associated with the first variation of the cylinder reference surface displacements in the axial, circumferential, and radial directions, $u(x,\theta)$, $v(x,\theta)$, and $w(x,\theta)$, respectively. The Ns and Ms with subscripts x and θ are the force and moment resultants, and $N_{\rm cr}$ is the sought-after critical, or buckling, load. For the problem here, the first variations of the force and moment resultants are given by

$$\begin{aligned} N_{x1} &= A_{11}\left(\frac{\partial u_1^o}{\partial x} + \beta_x^o\beta_{x1}^o\right) + A_{12}\left(\frac{\partial v_1^o}{R\partial\theta} + \beta_\theta^o\beta_{\theta 1}^o + \frac{w_1^o}{R}\right) \\ N_{\theta 1} &= A_{12}\left(\frac{\partial u_1^o}{\partial x} + \beta_x^o\beta_{x1}^o\right) + A_{22}\left(\frac{\partial v_1^o}{R\partial\theta} + \beta_\theta^o\beta_{\theta 1}^o + \frac{w_1^o}{R}\right) \\ N_{x\theta 1} &= A_{66}\left(\frac{\partial v_1^o}{\partial x} + \frac{\partial u_1^o}{R\partial\theta} + \beta_x^o\beta_{\theta 1}^o + \beta_\theta^o\beta_{x1}^o\right) \\ M_{x1} &= D_{11}\frac{\partial\beta_{x1}^o}{\partial x} + D_{12}\frac{\partial\beta_{\theta 1}^o}{R\partial\theta} + D_{16}\left(\frac{\partial\beta_{\theta 1}^o}{\partial x} + \frac{\partial\beta_{x1}^o}{R\partial\theta}\right) \\ M_{\theta 1} &= D_{12}\frac{\partial\beta_{x1}^o}{\partial x} + D_{22}\frac{\partial\beta_{\theta 1}^o}{R\partial\theta} + D_{26}\left(\frac{\partial\beta_{\theta 1}^o}{\partial x} + \frac{\partial\beta_{x1}^o}{R\partial\theta}\right) \\ M_{x\theta 1} &= D_{16}\frac{\partial\beta_{x1}^o}{\partial x} + D_{26}\frac{\partial\beta_{\theta 1}^o}{R\partial\theta} + D_{66}\left(\frac{\partial\beta_{\theta 1}^o}{\partial x} + \frac{\partial\beta_{x1}^o}{R\partial\theta}\right) \end{aligned} \tag{A2}$$

The rotations and the first variations of the rotations are defined as

$$\begin{aligned} &\beta_x^o = -\frac{\partial w^0}{\partial x}; \qquad \beta_\theta^o = -\frac{\partial w^o}{R\partial\theta}; \\ &\beta_{x1}^o = -\frac{\partial w_1^o}{\partial x}; \quad \text{and} \quad \beta_{\theta 1}^o = -\frac{\partial w_1^o}{R\partial\theta} \end{aligned} \tag{A3}$$

The variations in the displacements are taken to be of the form

$$\begin{aligned} &u_1^0 = U\cos\left(\frac{m\pi}{L}x\right)\cos(n\theta) \qquad v_1^0 = V\sin\left(\frac{m\pi}{L}x\right)\sin(n\theta) \\ &w_1^0 = W\sin\left(\frac{m\pi}{L}x\right)\cos(n\theta) \end{aligned} \tag{A4}$$

where U, V, and W are unknown constants. Substituting Eq. (A4) into Eqs. (A2) and (A3) then those results into Eq. (A1) and carrying out the spatial integrations results in three homogeneous equations from which to solve for the constants U, V, and W. To have a nontrivial solution results in an eigenvalue problem for $N_{\rm cr}$ in terms of the cylinder geometry and material properties. The multiplicity of critical loads is given by

$$N_{\rm cr}\left(\frac{m\pi}{L}\right) = T_{33} + \frac{2T_{12}T_{13}T_{23} - T_{11}T_{23}^2 - T_{22}T_{13}^2}{T_{11}T_{22} - T_{12}^2} \tag{A5}$$

where

$$\begin{aligned} T_{11} &= A_{11}\left(\frac{m\pi}{L}\right)^2 + A_{66}\left(\frac{n}{R}\right)^2 \\ T_{12} &= (A_{12} + A_{66})\left(\frac{m\pi}{L}\right)\left(\frac{n}{R}\right) \\ T_{13} &= \frac{A_{12}}{R}\left(\frac{m\pi}{L}\right) \\ T_{22} &= A_{66}\left(\frac{m\pi}{L}\right)^2 + A_{22}\left(\frac{n}{R}\right)^2 \\ T_{23} &= \frac{A_{22}}{R}\left(\frac{n}{R}\right) \\ T_{33} &= D_{11}\left(\frac{m\pi}{L}\right)^4 + (2D_{12} + 4D_{66})\left(\frac{m\pi}{L}\right)^2\left(\frac{n}{R}\right)^2 \\ &\quad + D_{22}\left(\frac{n}{R}\right)^4 + A_{22}\left(\frac{1}{R}\right)^2 \end{aligned} \tag{A6}$$

The values of m and n that result in the minimum value of the critical load can be determined. The critical value of axial strain is defined as

$$\varepsilon_{\rm cr} = -\frac{N_{\rm cr}}{A_{\rm eff}} \tag{A7}$$

where the effective axial stiffness $A_{\rm eff}$ is given as

$$A_{\text{eff}} = A_{11} - \frac{A_{12}^2}{A_{22}} \tag{A8}$$

Acknowledgment

This paper is dedicated to Professor Liviu Librescu, who served on the Ph.D. advisory committee of the first author, and who was killed in a classroom on April 16, 2007, while desperately saving the lives of the students.

References

[1] Soldatos, K. P., "Mechanics of Cylindrical Shells with Noncircular Cross Section: A Survey," *Applied Mechanics Reviews*, Vol. 52, No. 8, 1999, pp. 237–274.

[2] Sheinman, I., and M. Firer, "Buckling Analysis of Laminated Cylindrical Shells with Arbitrary Noncircular Cross Section," *AIAA Journal*, Vol. 32, No. 3, 1994, pp. 648–654.

[3] Sun, G., "Buckling and Initial Post-Buckling Behavior of Laminated Oval Cylindrical Shells Under Axial Compression," *Journal of Applied Mechanics*, Vol. 58, No. 3, 1991, pp. 848–851.

[4] Soldatos, K. P., and Tzivanidis, G. J., "Buckling and Vibration of Cross-Ply Laminated Noncircular Cylindrical Shells," *Journal of Sound and Vibration*, Vol. 82, No. 3, 1982, pp. 425–434.

[5] Soldatos, K. P., "Nonlinear Analysis of Transverse Shear Deformable Laminated Composite Cylindrical Shells Part II: Buckling of Axially Compressed Cross-Ply Circular and Oval Cylinders," *Transactions of the American Society of Mechanical Engineers, Journal of Pressure Vessel Technology*, Vol. 114, No. 1, 1992, pp. 110–114.

[6] Meyers, C. A., and Hyer, M.W., "Response of Elliptical Composite Cylinders to Internal Pressure Loading," *Mechanics of Composite Materials and Structures*, Vol. 4, No. 4, 1997, pp. 317–343.

[7] Firer, M., and Sheinman, I., "Nonlinear Analysis of Laminated Noncircular Cylindrical Shells," *International Journal of Solids and Structures*, Vol. 32, No. 10, 1995, p. 1405–1416. doi:10.1016/0020-7683(94)00191-X

[8] Meyer, C. A., and Hyer, M. W., "Response of Elliptical Composite Cylinders to Axial Compression Loading," *Mechanics of Composite Materials and Structures*, Vol. 6, No. 2, 1999, pp. 169–194.

[9] Sun, M., and Hyer, M. W., "Axial Buckling Behavior of Noncircular Composite Cylinders," *Proceedings of the American Society for Composites 20th Annual Technical Conference*, edited by F. K. Ko, G. R. Palmese, Y. Gogotsi, andA. S. D. Wang, [CD-ROM], DesTECH Publications, Inc., Lancaster, PA, 2005, ISBN 1-932078-50-9.

[10] Hyer, M. W., and McMurray, J. M., "Internally Pressurized Elliptical Composite Cylinders," *Composite Structures*, Vol. 46, No. 1, 1999, pp. 17–31. doi:10.1016/S0263-8223(99)00038-0

[11] Hyer, M. W., and Vogl, G. A., "Response of Elliptical Composite Cylinders to a Spatially Uniform Temperature Change," *Composite Structures*, Vol. 51, No. 2, 2001, pp. 169–179. doi:10.1016/S0263-8223(00)00142-2

[12] McMurray, J. M., and Hyer, M. W., "Response and Failure of Internally Pressurized Elliptical Composite Cylinders," *Journal of Thermoplastic Composite Materials*, Vol. 14, No. 5, 2001, pp. 433–445.

[13] McMurray, J. M., and Hyer, M. W., "Response and Failure Characteristics of Internally Pressurized Elliptical Composite Cylinders," *AIAA Journal*, Vol. 40, No. 1, 2002, pp. 117–125.

[14] Wolford, G. F., and Hyer, M. W., "Failure Initiation and Progression in Internally Pressurized Elliptical Composite Cylinders," *Mechanics of Advanced Materials and Structures*, Vol. 12, No. 6, 2005, pp. 437–455. doi:10.1080/15376490500259269

[15] Haynie, W. T., and Hyer, M. W., "Behavior of Elliptical Composite Cylinders in Torsion," AIAA Paper 2006-1648, 2006.

[16] Thomsen, O. T., and Vinson, J. R., "Analysis and Parametric Study of Noncircular Pressurized Sandwich Fuselage Cross Section Using a High-Order Sandwich Theory Formulation," *Journal of Sandwich Structures and Materials*, Vol. 3, No. 3, 2001, pp. 220–250.

[17] Thomsen, O. T., and Vinson, J. R., "Conceptual Design Principles for Noncircular Pressurized Sandwich Fuselage Sections: A Design Study Based on a High-Order Sandwich Theory Formulation," *Journal of Composite Materials*, Vol. 36, No. 3, 2002, pp. 313–345. doi:10.1177/0021998302036003468

[18] Preissner, E. C., and Vinson, J. R., "Unique Bending Boundary Layer Behaviors in a Composite Noncircular Cylindrical Shell," *Composites. Part B, Engineering*, Vol. 35, No. 3, 2004, pp. 223–233.

[19] Heck, O. S., "The Stability of Orthotropic Elliptical Cylinders in Pure Bending," NACA TM No. 834, 1937

[20] Riddick, J. C., and Hyer, M. W., "The Response of Segmented-Stiffness Composite Cylinders to Axial Endshortening," *Composite Structures*, Vol. 40, No. 2, 1997, pp. 103–114. doi:10.1016/S0263-8223(97)00143-8

[21] Riddick, J. C., and Hyer, M. W., "Internal Pressure Loading of Segmented-Stiffness Composite Cylinders," *Composite Structures*, Vol. 45, No. 4, 1999, pp. 311–320. doi:10.1016/S0263-8223(99)00037-9

[22] Riddick, J. C., and Hyer, M. W., "Postbuckling Behavior of Segmented Circular Composite Cylinders," *AIAA Journal*, Vol. 42, No. 1, 2004, pp. 185–195.

[23] Hyer, M. W., *Stress Analysis of Fiber-Reinforced Composite Materials*, WCB/MCGraw–Hill, New York, 1998, pp. 355–357.

[24] Kempner, J., and Chen, Y.-N., "Buckling and Postbuckling of an Axially Compressed Oval Cylindrical Shell," *Proceedings: Symposium on Theory of Shells to Honor Lloyd Hamilton Donnell*, edited by D. Muster, University of Houston McCutchan Publishing Corporation, 1967, pp. 141–175.

A. Palazotto
Associate Editor